Exploring the dynamic behavior of the two-phase model in radiative non-Newtonian nanofluid flow with Hall current and ion slip effects

Q6 The corrections made in this section will be reviewed and approved by a journal production editor.

Mohammad Akram[a], akramkhan_20@rediffmail.com, Osama Ala'yed[b], alayedo@jadara.edu.jo, Rania Saadeh[c], rsaadeh@zu.edu.jo, Ahmad Qazza[c], aqazza@zu.edu.jo, A.M. Obalalu[d,*], adebowale.obalalu17@gmail.com, Umair Khan[e,f,**], umairkhan@sakarya.edu.tr, Adil Darvesh[g], adildarvesh@hu.edu.pk, A.A. Usman[h], abdulazeez.usman@fuhsi.edu.ng, A.M. Abdul-Yekeen[i], mayowaabideen@gmail.com, Syed Modassir Hussain[a], Q1 syed.hussain@iu.edu.sa

[a]Department of Mathematics, Faculty of Science, Islamic University of Madinah, Madinah, 42351, Saudi Arabia

[b]Department of Mathematics, Jadara University, Irbid, 21110, Jordan

[c]Department of Mathematics, Faculty of Science, Zarqa University, Zarqa, 13110, Jordan

[d]Department of Mathematics and Statistics, Kwara State University, Malete, Nigeria

[e]Department of Mathematics, Faculty of Science, Sakarya University, Serdivan, Sakarya, 54050, Turkey

[f]Department of Mechanics and Mathematics, Western Caspian University, Baku, 1001, Azerbaijan

[g]Department of Mathematics and Statistics Hazara University Mansehra, 21300, Pakistan

Q2 [h]Department of Physical and Chemical Sciences, Federal University of Health Sciences Ila-Orangun, Nigeria

[i]Department of Mathematics, Lamar University Beaumont Texas, USA

*Corresponding author.

**Corresponding author. Department of Mathematics, Faculty of Science, Sakarya University, Serdivan, Sakarya, 54050, Turkey.

Abstract

The utilization of Hall current and ion slip in electrically conducting fluids has garnered significant attention, especially in applications like magnetohydrodynamic (MHD) power generation and electrochemical sensors in industrial plasma processes. These phenomena have become key focuses for scientists and engineers seeking innovative solutions to enhance productivity and sustainability in the manufacturing industry. This study investigates the steady three-dimensional flow dynamics of a magnetohydrodynamic Casson nanofluid over an exponentially stretching sheet, influenced by Hall current and ion slip. The analysis incorporates the effects of multiple slips, as well as heat transport in a rotating system, accounting for solar radiation, viscous-Ohmic dissipation, and slip effects. This kind of flow problem has numerous applications across various scientific and engineering fields, including MHD generators, Hall thrusters, thermal energy storage systems, electronic cooling, and spacecraft design. The governing equations are altered into ordinary differential equations which are then solved using Gegenbauer wavelets collocation-based techniques. Moreover, the study reveals that increasing Hall current and ion slip enhances velocity distribution, while the thermal transport rate significantly increases with improved solar radiation.

Keywords:

Magnetohydrodynamic; Casson flow; Nanofluid; Solar radiation mechanism; Hall current and ion slip effects

The table layout displayed in this section is not how it will appear in the final version. The representation below is solely purposed for providing corrections to the table. To view the actual presentation of the table, please click on the Preview located at the top of the page.

Nomenclature

Nt	Thermophoresis parameter
Pr	Prandtl number
M	Magnetic parameter
C_R	Chemical reaction parameter
S_c	Schmidt number
N^*	The ratio of concentration to thermal buoyancy forces
ω_c	Dimensionless temperature jumps parameters
E_1	Activation energy parameter
ς_1	Quadratic convection parameters for temperature
ω_a	Velocity slip parameters
K_R	Rotation parameter
$Gr_{\tilde{x}}$	Thermal Grashof number
$Gc_{\tilde{x}}$	Solutal Grashof number
Q_N	Heat generation parameter
χ_r	Temperature ratio parameter
E_c	Eckert number
ς_2	Quadratic convection parameters for concentration
A_v	Velocity ratio parameter
R_N	Solar radiation parameter
$Re_{\tilde{X}}$	Local Reynolds numbers
ω_b	Velocity slip parameters
λ_a	Mixed convection parameter
Nb	Brownian motion parameter
$\tilde{A}_w$, $\tilde{B}_w$	stretching velocities
α_e	Ion slip
$\tilde{\psi}_w$ *and* $\tilde{\phi}_w$	temperature and concentration
N_1 and N_2	Velocity slip coefficients

μ	dynamic viscosity
g	gravitational acceleration

1 Introduction

Q3 Hall currents are a fundamental concept in physics and engineering, first introduced by the renowned American physicist Edwin Hall in 1879. This phenomenon mostly occurs by applying an external magnetic field perpendicular to the direction of the electric current flowing through the conductive materials i.e. metals and semiconductors. The applied magnetics force causes a deflection in the moving charge carriers (electrons) in the conductor, which enables charge accumulation on one side of the conductor, resulting in an electric field that opposes the flow of current and develops a voltage difference called Hall voltage. The Hall effects mostly occur in electrically conductive liquids substances, specifically Hall effect in fluid dynamics is characterized by the transverse voltage differential (TVD) that occurs across a conductor when it is subjected to a magnetic field that runs counter to the direction of fluid flow. The phenomena (Hall forces) are a great area of interest because it is widely used in various applications such as the characterization of semiconductors, magnetic field sensing, density, and sign measuring of charge in material. More generally Hall effect in the context of fluid flow is an interesting phenomenon with applications in many technical and scientific fields. Hall (Hall, 1988) studied the turbulent flow to measure the effect of mean forces near to the boundaries. Mollinger et al. (Nimmy et al., 2024) considered a uniform flow in the viscous sublayer of a turbulent boundary layer to calculate the lift force exerted on a particle. It is worth noting that several factors such as magnetic field orientation, strength of field, and fluid conductivity are very important in better understanding of Hall voltage in fluid flow (Al-Turef et al., 2024). The Rheology of gyrotactic microorganisms in Jeffrey fluid flow was examined by (Sarfraz & Khan, 2024). Heat transfer in Jeffrey fluid flow over a power law lubricated surface inspired by solar radiations and magnetic flux was examined by (Ahmed et al., 2023). Significance of Buongiorno's model on viscoelastic MHD flow over a heated lubricated surface subject to Joule heating were study by (Sarfraz et al., 2023). Forced convection in 3D Maxwell nanofluid flow via Cattaneo–Christov theory with Joule heating was studied by (Ahmed et al., 2021). Hall effect can be used in industrial work to monitor rate of flow in conductive fluid devices such as flow meters. Paun et al. (Paun et al., 2013) used this idea to design Hall-based sensors and conducted a behavioral analysis on them. The Non-axisymmetric Homann stagnation-point flow of Walter's B nanofluid over a cylindrical disk was studied by (Khan et al., 2020). The viscoelastic nanofluid motion for the Homann stagnation region with thermal radiation characteristics was studied by (Khan et al., 2021). Other important ideas are summarized in the following research (Roja et al., 2024; Vinothkumar et al., 2024).

Chemical reactions are basic processes in which reactants are used to form different products under some chemical transformations. Generally, this process involves breaking and forming chemical bonds and producing changes properties of the substances. It is very essential to know about some prominent factors which can influence reaction rates such as catalysts, temperature, and concentration. The knowledge of chemical reactions is crucial in many fields, including chemistry, environmental, biological sciences, and computational fluid dynamics, specifically, they also perform a significant role in fluid flow processes in various ways such as heat transfer, energy generation, fluid composition, chemical mixing of particles in fluid as well as erosion and corrosion. In general, it is a fundamental process to manipulate and understand fluid flow processes. Knowledge of chemical kinetics, thermodynamics, and transport phenomena is a pathway to efficiently assessing and optimizing fluid flow systems involving chemical reactions. Venkatachalam (Venkateswarlu & Narayana, 2015) studied the viscous elastic fluid under the influence of magnetohydrodynamics (MHD) accompanied by chemical reactions in a moveable vertical surface. They observed the role of chemical reactions in the rheology of fluid and determined how viscous-elastic fluid swift the flow characteristics. Salawu et al. (Salawu et al., 2023) discussed chemical reactions together with MHD in a flow process over a stretching nonlinear-permeable sheet. Additionally, they introduced the idea of slip consequences in a chemically characterized flow to improve the flow process for a smooth heat transfer. Furthermore, a comprehensive study of the mass and heat transport mechanisms in a chemically characterized flow driven by a moving vertical plate was conducted by Rout et al. (Rout et al., 2013). Zeeshan et al. (Zeeshan et al., 2021) worked on non-Newtonian nanofluid using the catalytic chemical reaction over a parabolic surface for analysis of energy generation and its utility in practical scenarios. In the context of fluid flow phenomena, the role of activation energy is superficial because its importance is profound and can be understood in many situations, including temperature sensitivity, autocatalysis, reaction rate

control, safety considerations, product selection, and process optimization. Understanding activation energy is essential for better predictions of the reactions involved in optimizing process efficiency and controlling heat transfer. Paul et al. (Paul et al., 2023) conducted a numerical simulation to investigate the mass and heat transfer characteristics of Maxwell nanofluids using an unstable horizontal cylinder. Their study took into account the effects of Arrhenius activation energy and variable thermal conductivity. Mustafa et al. (Mustafa et al., 2017) investigated the behavior of nanofluid flow along a vertical surface, considering the impact of buoyancy effects on magnetohydrodynamic (MHD) flow that involves chemical reactions and activation energy. In addition, the subsequent research conducted by the author (Li et al., 2024; Ramesh, Saadeh, et al., 2024) highlighted the importance of induced magnetic fields, chemical reactions, and Arrhenius activation energy.

The non-Newtonian fluid models are utilized to describe the non-Newtonian nature of fluids whose viscosity varies with the rate of shear stress. Amongst these non-Newtonian models, one of the well-known models is the Casson model which is associated with yield stress. They play a key role in many real applications including, biomedical, heat transfer, and lubricants. Singh et al. (Singh et al., 2024) discussed Casson fluid with hybrid nanoparticles using multiple geometries such as plate, cone, and wedge for deep analysis of the thermal transportation process under the action of magnetic effect. Shoaib et al. (Shoaib & Javed, 2024) discussed the thermal convective mechanism in a Casson-fluid over a cylindrical region. They discussed the natural convective heat transfer along with magnetohydrodynamics (MHD) influence. Fluid flow with slip consequences is an interesting domain of fluid dynamics which accounts for the relative motion between the boundary of the surface and the fluid, which is very essential in several advanced applications. It is worth noting that modeling and understanding this behavior allows for good optimization and precise control in scientific and many engineering applications particularly relevant in micro and nanofluidic. Sekhar et al. (Raja Sekhar et al., 2024) studied the Casson nanofluid over a heated expanded surface to investigate the heat transport mechanism utilizing thermal radiation in the presence of variable effects such as slips and wall thickness of nanofluid flow. The significance of heat transfer is very crucial in many industrial processes where fluid-based systems are used to optimize heat transport. Mehmood et al. (Mahmood et al., 2024) made some numerical computations of heat transportation in Casson-nanofluid over a moved heated surface in the presence of chemical reactions and mixed convection. Additionally, the flow was subjected to thermal slip consequences accompanied by velocity influence. The findings of their study suggest enhanced heat transportation due to multiple slip phenomena in a Casson fluid flow.

Rotatory fluid flow with nonlinear convection is a complex phenomenon encountered in many areas, such as astrophysics, engineering, and geophysical fluid dynamics. Due to its large practical implications, it is very essential to have a better understanding of nonlinear convection in rotating systems. It requires a blend of computational, theoretical, and experimental approaches to fully predict and capture the complex behavior of such fluidic systems. Many researchers focused on these phenomena and presented many novel ideas. Ullah et al. (Ullah et al., 2023) presented a thin film study of trihybrid nanofluid in the rotatory system with nonlinear convection and magnetic field. Kanwal et al. (Kanwal et al., 2023) studied heat and mass transport phenomenon in nanofluid flow over the rotating disk under the influence of using thermal radiation, and activation rate along with linear/nonlinear mixed convection. Sharma et al. (Sharma & Yadav, 2023) presented a theory of rotatory and internal heat sink source effect due to linear/nonlinear phenomenon on Bénard convection. Furthermore, linear and weakly nonlinear analysis of a viscoelastic binary fluid flow through a porous surface with the combined effect of rotation and helical effect is discussed by Kpossa and Monwanou (Kpossa & Monwanou, 2023). Moreover, the same investigation for the thermal stability of magnetized Newtonian nanofluid in a rotating frame was conducted by Rana et al. (Rana & Khurana, 2023). One of the major concerns in a rotatory flow is viscous ohmic dissipation which refers to the process of conversion of electrical energy into heat due to the resistive forces (viscous) in a rotating conductive fluid. This process is significant in numerous scientific and engineering applications, such as in astrophysics, geophysics, as well as in industrial processes. This phenomenon (viscous ohmic dissipation in rotary fluid flow) requires a multidisciplinary approach, combining electromagnetism, thermal physics, and fluid dynamics knowledge and it is smoothly used for good prediction and optimizing the behavior of systems involving rotating conductive fluids. Vardagala et al. (Vardagala et al., 2024) discussed the combined effect (Viscous dissipation & Ohmic heating) in a hydromagnetic peristaltic flow of a Casson nanofluid utilizing the vertical porous channel. Butt et al. (Butt et al., 2024) studied unsteady Casson nanofluid by focusing thermal radiation and Ohmic dissipation via an intelligent computing paradigm to explore the Casson flow characteristics under the influence of magnetic effect. Ram et al. (Ram et al., 2023) studied 2D Casson flow under the influence of Ohmic dissipation for the analysis of Cross-Diffusion and uneven heat source/sink effect on the flow through an infinite plate. Furthermore, Li et al. (Li et al., 2023) presented a novel entropy model for radiative time-

dependent flow. They considered radiative time-dependent flow under the influence of some prominent facts such as chemical reactions, viscous dissipation, and Ohmic heating to analyze mass and thermal transportation. Computational analysis on radiative non-Newtonian Carreau nanofluid flow in a microchannel under magnetic properties was examined by (Ramesh et al., 2023). Hybrid-nanofluid magneto-convection flow and porous media contribution to entropy generation were examined by (Mebarek-Oudina et al., 2024). The role of quadratic-linearly radiating heat source with Carreau nanofluid and exponential space-dependent past a cone and a wedge for medical engineering application were examined by (Mebarek-Oudina et al., 2023). The mathematical background of fluid dynamics and nanofluids was examined by (Ramesh et al., 2024b). Moreover, the following research (Gasmi et al., 2024a, 2024b; Obalalu et al., 2024) emphasizes the phenomenon of viscous ohmic dissipation in rotary fluid flow.

1.1 Purpose of the present study

1.1.1 Existing literature

Numerous analytical and numerical studies conducted in recent years have examined boundary layer flow, heat transfer, mass transfer analysis, and rotating Casson fluids over an exponentially elongating sheet. These studies focus on nanoparticle concentration that undergoes binary chemical reactions and include the effects of Hall current and ion slip. Several researchers have studied fluids characterized by combined slip conditions at the surface boundary, such as wedge-shaped channels, curved expanding surfaces, stretching sheets, and Poiseuille flow, and they have evaluated the solutions to these problems.

1.1.2 Research gap

Based on the previously discussed literature and current studies, there has been no attempt to investigate the influence of Hall and ion slip over an exponentially elongating sheet with nonlinear thermal radiation. The existing literature does not include any attempts to create a model that incorporates rotating Casson nanofluid flow. The focus of this study is to examine the solutions for the flow of rotating Casson nanofluid flow influenced by Hall and ion slip effects, while also considering the quadratically varying heat and mass convections.

1.1.3 Novel aspects

This research study includes various innovative elements that enhance its originality and importance. The unique contribution of this study is outlined below.

- The Hall current and ion slip are explored to estimate and enhance the precision of thermal systems, which is essential for applications at high temperatures plasmas.
- The study explores quadratically varying heat and mass convections by considering the cyclotron frequency and electron collision time with multiple slips at the boundary surface.
- The model considers the magnetohydrodynamics Casson nanofluid flow as well as Arrhenius activation energy with binary chemical reaction.
- The viscous dissipation with solar radiation mechanism phenomenon is also considered.
- The comparative investigation of three-dimensional steady flow with an internal heat source on the hydrodynamic and thermal boundary layer is examined.
- The new Gegenbauer wavelet method, with the help of MATHEMATICA software, is utilized to achieve robust and accurate numerical outcomes.
- This research has important implications for several scientific and engineering applications, such as chemical engineering, hydroelectric, chemical energy, pharmaceutical manufacturing, biofuel production, and wastewater treatment.

1.1.4 problem statement

Non-Newtonian nanofluids are increasingly being used in advanced engineering and industrial applications due to their enhanced thermal properties and unique rheological behavior. The incorporation of nanomaterials into a non-

Newtonian base fluid result in a complex interaction between the fluid's viscosity, thermal conductivity, and other thermophysical properties. In many applications, such as in cooling systems, energy generation, and biomedical devices, understanding the influence of external forces such as magnetic fields are crucial. The Hall current and ion slip are electromagnetic phenomena that can significantly affect the behavior of charged particles in a fluid. The Hall effect refers to the generation of a transverse electric field due to the movement of charged particles under the influence of a magnetic field, while ion slip accounts for the relative movement between ions and neutral particles in the fluid. Both phenomena can alter the momentum and energy equations, leading to changes in fluid flow and heat transfer rates.

2 Mathematical description of the problem

Let us consider the three-dimensional dynamics of a non-Newtonian Casson nanofluid under the influence of magnetohydrodynamics (MHD) as it flows over an exponentially stretching sheet, characterized by nonlinear convection and the combined effects of viscous and Ohmic dissipation. Fig. 1a reveals a schematic representation showing that the sheet is positioned at $\tilde{z} = 0$, while the velocity flow is restricted to the area where $\tilde{z} \geq 0$. The velocities at which the wall stretches along the $\tilde{x}$ and $\tilde{y}$ directions are denoted as $\tilde{A}_w$ and $\tilde{B}_w$, respectively. The sheet rotates about the $\tilde{z}$-axis, exhibiting an angular speed defined via the $\Omega^* = \Omega_0 \exp\left(\frac{\tilde{x}+\tilde{y}}{L}\right)$, whereas $B = \mathrm{B}_0 \exp\left(\frac{\tilde{x}+\tilde{y}}{L}\right)$ defined the variable magnetic field. Here, B_0 and Ω_0 represents the uniform magnetic and uniform angular velocity, respectively. It is presumed that $\tilde{\psi}_w$ and $\tilde{\phi}_w$ refer to the wall temperature and concentration, respectively. The flow field is not subjected to an external electric field, thereby excluding polarization effects. The magnetic Reynolds number is low enough to assume that any induced magnetic field is negligible. The solar-radiative is included through the application of the Rosseland thermal flux model. The velocity slip, temperature, and concentration jump at the surface boundary are taken into account. Fig. 1b display the applications of the requisite posited nanofluid (Ramesh et al., 2024b).

Images may appear blurred during proofing as they have been optimized for fast web viewing. A high quality version will be used in the final publication. Click on the image to view the original version.

alt-text: Fig. 1a

Fig. 1a

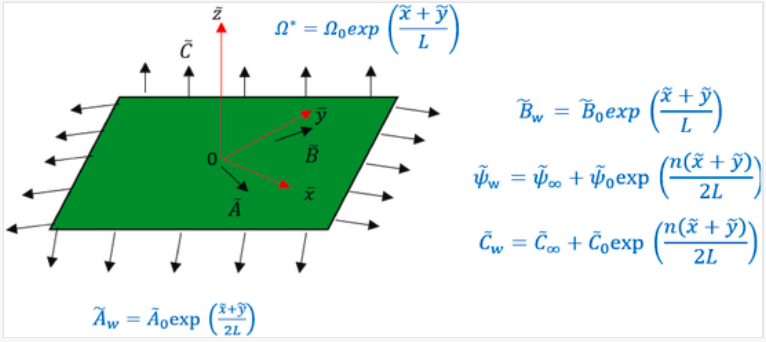

Schematic representation of the problem.

Images may appear blurred during proofing as they have been optimized for fast web viewing. A high quality version will be used in the final publication. Click on the image to view the original version.

alt-text: Fig. 1b

Fig. 1b

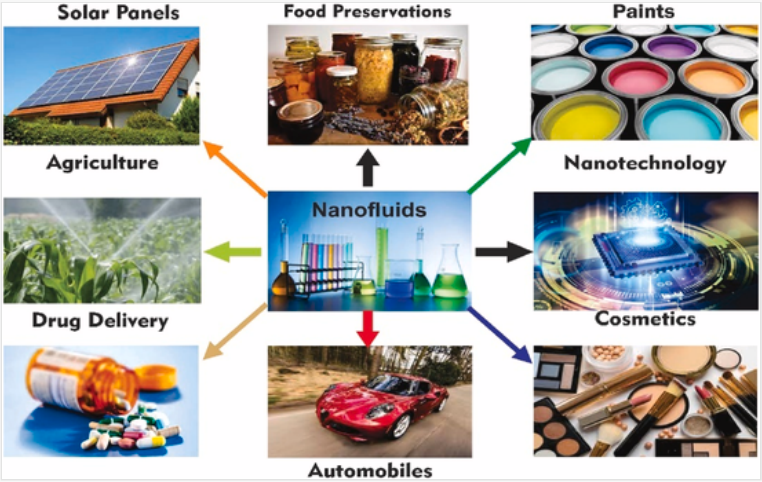

Applications of the requisite posited nanofluid.

The frequency of electron-atom collisions is considered to be very high, which means that Hall and ion slip currents must be taken into account and cannot be ignored. When the intensity of the magnetic field is significant, the generalized form of Ohm's law can be expressed as:

$$J = \sigma\left(E + V \times B^{*}\right) - \frac{\omega_e \tau_e}{B}\left(J + B^{*}\right) + \frac{\omega_e \tau_e \xi_b}{B^2}\left(\left(J \times B^{*}\right) \times B^{*}\right) = 0, \tag{1}$$

where E is called the electric field, B^{*} is the magnetic field vector, V is the velocity field vector, ω_e is the Cyclotron frequency and τ_e is the electron collision time.

2.1 The governing equations of the problem

Based on the previously mentioned assumption regarding MHD Casson nanofluid, the governing equations can be expressed as follows (Gasmi, Obalalu, Akindele, et al., 2024; Obalalu et al., 2024):

$$\frac{\partial \widetilde{A}}{\partial \widetilde{x}} + \frac{\partial \widetilde{B}}{\partial \widetilde{y}} + \frac{\partial \widetilde{C}}{\partial \widetilde{z}} = 0, \tag{2}$$

$$\begin{aligned}\widetilde{A}\frac{\partial \widetilde{A}}{\partial \widetilde{x}} + \widetilde{B}\frac{\partial \widetilde{A}}{\partial \widetilde{y}} + \widetilde{C}\frac{\partial \widetilde{A}}{\partial \widetilde{z}} - 2\Omega^{*}\widetilde{B} &= v\left(1 + \frac{1}{\beta}\right)\frac{\partial^2 \widetilde{A}}{\partial \widetilde{z}^2} + \frac{\sigma B^2}{\rho_f\left(\alpha_e^2 + \xi_a^2\right)}\left(\xi_a \widetilde{B} - \alpha_e \widetilde{A}\right) \\ &+ \left\{g\alpha_1\left(\widetilde{\psi} - \widetilde{\psi}_{\infty}\right) + g\alpha_2\left(\widetilde{\psi} - \widetilde{\psi}_{\infty}\right)^2\right\} + \left\{g\beta_1\left(\widetilde{\phi} - \widetilde{\phi}_{\infty}\right) + g\beta_2\left(\widetilde{\phi} - \widetilde{\phi}_{\infty}\right)^2\right\},\end{aligned} \tag{3}$$

$$\widetilde{A}\frac{\partial \widetilde{B}}{\partial \widetilde{x}} + \widetilde{B}\frac{\partial \widetilde{B}}{\partial \widetilde{z}} + \widetilde{C}\frac{\partial \widetilde{B}}{\partial \widetilde{z}} + 2\Omega^{*}\widetilde{A} = v\left(1 + \frac{1}{\beta}\right)\frac{\partial^2 \widetilde{B}}{\partial \widetilde{z}^2} - \frac{\sigma B^2}{\rho_f\left(\alpha_e^2 + \xi_a^2\right)}\left(\xi_a \widetilde{A} + \alpha_e \widetilde{B}\right), \tag{4}$$

$$\widetilde{A}\frac{\partial \widetilde{\psi}}{\partial \widetilde{x}} + \widetilde{B}\frac{\partial \widetilde{\psi}}{\partial \widetilde{z}} + \widetilde{C}\frac{\partial \widetilde{\psi}}{\partial \widetilde{z}} = \alpha^{*}\frac{\partial^2 \widetilde{\psi}}{\partial \widetilde{z}^2} + \tau\left\{D_B\left(\frac{\partial \widetilde{\phi}}{\partial \widetilde{z}}\right) + \frac{D_{\widetilde{\psi}}}{\widetilde{\psi}_{\infty}}\left(\frac{\partial \widetilde{\psi}}{\partial \widetilde{z}}\right)\right\}\frac{\partial \widetilde{\psi}}{\partial \widetilde{z}} + \frac{\sigma B^2}{\left(\rho c_p\right)_f}\left(\widetilde{A}^2 + \widetilde{B}^2\right) - \frac{1}{\left(\rho c_p\right)_f}\frac{\partial q_r}{\partial \widetilde{z}} + \frac{\mu}{\left(\rho c_p\right)_f}\left(1 + \right. \tag{5}$$

$$\widetilde{A}\frac{\partial \widetilde{\phi}}{\partial \widetilde{x}} + \widetilde{B}\frac{\partial \widetilde{\phi}}{\partial \widetilde{y}} + \widetilde{C}\frac{\partial \widetilde{\phi}}{\partial \widetilde{z}} = D_B\frac{\partial^2 \widetilde{\phi}}{\partial \widetilde{z}^2} + \frac{D_{\widetilde{\psi}}}{\widetilde{\psi}_{\infty}}\frac{\partial^2 \widetilde{\psi}}{\partial \widetilde{z}^2} - K_1^2\left(\widetilde{\phi} - \widetilde{\phi}_{\infty}\right)\left(\frac{\widetilde{\psi}}{\widetilde{\psi}_{\infty}}\right)^{n^{*}} exp\left(-\frac{E_a}{k_1^{*}\widetilde{\psi}}\right), \tag{6}$$

The slip conditions are:

$$\begin{aligned}
\widetilde{A} &= \widetilde{A}_w + \widetilde{A}_{slip} = \widetilde{A}_w + \left(1+\frac{1}{\beta}\right) N_1 \mu \frac{\partial \widetilde{A}}{\partial \widetilde{z}}, \\
\widetilde{B} &= \widetilde{B}_w + \widetilde{B}_{slip} = \widetilde{B}_w + \left(1+\frac{1}{\beta}\right) N_2 \mu \frac{\partial \widetilde{B}}{\partial \widetilde{z}}, \\
\widetilde{C} = 0, \widetilde{\psi} &= \widetilde{\psi}_w + d_1 \left(\frac{\partial \widetilde{\psi}}{\partial \widetilde{z}}\right), \widetilde{\phi} = \widetilde{\phi}_w + d_2 \left(\frac{\partial \widetilde{\phi}}{\partial \widetilde{z}}\right), \text{at } \widetilde{z} = 0, \\
\widetilde{A} &\to 0, \widetilde{B} \to 0, \widetilde{\psi} \to \widetilde{\psi}_\infty, \widetilde{\phi} \to \widetilde{\phi}_\infty, \text{as } \widetilde{z} \to \infty.
\end{aligned} \tag{7}$$

Here, $\left(\widetilde{A}_w, \widetilde{B}_w\right)$ is the stretching velocities. $\alpha_e = 1 + \xi_a \xi_b$, where α_e is defined as an ion slip parameter. Furthermore, $\widetilde{\psi}_w$ and $\widetilde{\phi}_w$ are temperature and concentration at the surface of the sheet. Velocity slip coefficients are N_1 and N_2. Also, μ is the dynamic viscosity and g is the gravitational acceleration. According to references (Mustafa et al., 2017) and (Ram et al., 2023), the factors for Q_0, K_1, N_1, N_2, d_1, d_2 are defined as the variable heat generation coefficient $Q_0 = Q_1 \exp\left(\frac{\widetilde{x}+\widetilde{y}}{L}\right)$, the chemical reaction $K_1 = K_2 \exp\left(\frac{\widetilde{x}+\widetilde{y}}{2L}\right)$, the velocity slip factors $N_1 = N_3 \exp\left(-\frac{\widetilde{X}+\widetilde{Y}}{2L}\right)$, $N_2 = N_4 \exp\left(-\frac{\widetilde{X}+\widetilde{Y}}{2L}\right)$, and the thermal and solutal jump factors $d_1 = d_3 \exp\left(-\frac{\widetilde{X}+\widetilde{Y}}{2L}\right)$, $d_2 = d_4 \exp\left(-\frac{\widetilde{X}+\widetilde{Y}}{2L}\right)$.

2.2 Similarity variables and conversion of the governing equations

To ease the analysis of the given problem, the following similarity transformations are defined as (Li et al., 2024; Mustafa et al., 2017):

$$\begin{aligned}
\widetilde{C} &= -\sqrt{\frac{\nu \widetilde{A}_0}{2L}} exp\left(\frac{\widetilde{x}+\widetilde{y}}{2L}\right)\left(h + \vartheta h' + g + \vartheta g'\right), \\
\widetilde{B} &= \widetilde{A}_0 \, exp\left(\frac{\widetilde{x}+\widetilde{y}}{L}\right) g', \widetilde{A} = \widetilde{A}_0 \, exp\left(\frac{\widetilde{x}+\widetilde{y}}{L}\right) h', \\
\widetilde{\phi} &= \widetilde{\phi}_\infty + \widetilde{\phi}_0 \, exp\left\{\frac{n\left(\widetilde{x}+\widetilde{y}\right)}{2L}\right\} \chi, \\
\widetilde{\psi} &= \widetilde{\psi}_\infty + \widetilde{\psi}_0 \exp\left\{\frac{n\left(\widetilde{x}+\widetilde{y}\right)}{2L}\right\} \zeta, \\
\vartheta &= \widetilde{z}\sqrt{\frac{\widetilde{A}_0}{2\nu L}} exp\left(\frac{\widetilde{x}+\widetilde{y}}{2L}\right).
\end{aligned} \tag{8}$$

The variable introduced through the similarity transformation in the equation (8) transformed the flow problem into a corresponding system of ordinary differential equations (ODEs). Utilizing the expression in the equation (8), the equations from ((2) to ((6) can be transformed into the following set of ordinary differential equations:

$$\begin{aligned}
(h+g)h'' - 2\left(h'+g'\right)h' + \left(1+\frac{1}{\beta}\right)h''' + 4K_R g' + \frac{M}{\left(\alpha_e^2+\xi_a^2\right)}\left(\xi_a g' - \alpha_e h'\right) + \\
2\lambda_a \chi\left(1+\varsigma_1\chi\right) + 2\lambda_a N^* \zeta\left(1+\varsigma_2\zeta\right) = 0,
\end{aligned} \tag{9}$$

$$(h+g)g'' - 2\left(h'+g'\right)g' + \left(1+\frac{1}{\beta}\right)g''' - 4K_R h' - \frac{M}{\left(\alpha_e^2+\xi_a^2\right)}\left(\xi_a h' + \alpha_e g'\right) = 0, \tag{10}$$

$$\frac{1}{Pr}\chi'' + \frac{R_N\left\{1+\left(X_r-1\right)X\right\}^2}{Pr}\left[\left(\chi_r-1\right)\chi'^2 + \left\{1+\left(\chi_r-1\right)X\right\}\chi''\right] + (h+g)\chi' - n\left(h'+g'\right)\chi + Nt\chi'^2 + Nb\chi'\zeta' + \left(\tag{11}$$

$$\zeta'' - nS_c\left(h' + g'\right)\zeta + S_c\left(h + g\right)\zeta' + \frac{Nt}{Nb}\chi'' - C_R S_c \zeta\left(1+(\chi_r - 1)\,\chi\right)^{n^*}\ exp\left[-\frac{E_1}{(1+(\chi_r - 1)\,\chi)}\right] = 0. \quad (12)$$

The transformed boundary conditions are:

$$h\left(0\right) = 0, h'\left(0\right) = 1 + \left(1 + \frac{1}{\beta}\right)\omega_a h''\left(0\right), h'\left(\infty\right) \to 0, g\left(0\right) = 0, g'\ \left(0\right) = 1 + \left(1 + \frac{1}{\beta}\right)\ \omega_b\ g''\ \left(0\right), g'\ \left(\infty\right) \to 0, \chi\left(0\right) = 1 + \quad (13)$$

In above dimensionless equations involve distinct pertinent parameters which are mathematically and namely displayed in Table 1.

alt-text: Table 1

Table 1

The distinct pertinent parameters in the similarity equations.

Expressions	Descriptions	Expressions	Descriptions
$Nt = \frac{\tau D_{\widetilde{\psi}}\left(\widetilde{\psi}_w - \widetilde{\psi}_\infty\right)}{\nu\widetilde{\psi}_\infty}$	Thermophoresis parameter	$Gr_{\tilde{x}} = \frac{g\alpha_1\left(\widetilde{\psi}_w - \widetilde{\psi}_\infty\right)L^3}{\nu^2},$	Thermal Grashof number
$Pr = \frac{\nu}{\alpha^*}$	Prandtl number	$Gc_{\tilde{x}} = \frac{g\beta_1\left(\widetilde{\phi}_w - \widetilde{\phi}_\infty\right)L^3}{\nu^2}$	Solutal Grashof number
$M = \frac{2L\sigma B_0^2}{\rho_f \widetilde{A}_0}$	Magnetic parameter	$Q_N = \frac{2LQ_1}{\widetilde{A}_0\left(\rho c_p\right)_f}$	Heat generation parameter
$C_R = \frac{2LK_2^2}{\widetilde{A}_0}$	Chemical reaction parameter	$\chi_r = \frac{\widetilde{\psi}_w}{\widetilde{\psi}_\infty}$	Temperature ratio parameter
$S_c = \frac{\nu}{D_B}$	Schmidt number	$E_c = \frac{\mu\widetilde{A}_w^2}{\nu\left(\rho c_p\right)_f\left(\widetilde{\psi}_w - \widetilde{\psi}_\infty\right)}$	Eckert number
$N^* = \frac{Gr_{\tilde{x}}^*}{Gr_{\tilde{x}}}$	Ratio of concentration to thermal buoyancy forces	$\varsigma_2 = \frac{\left(\widetilde{\phi}_w - \widetilde{\phi}_\infty\right)\beta_2}{\beta_1}$	Quadratic convection parameters for concentration
$\omega_c = d_3\sqrt{\frac{\widetilde{A}_0}{2\nu L}}$	Dimensionless temperature jumps parameters	$A_v = \frac{\widetilde{B}_0}{\widetilde{A}_0}$	Velocity ratio parameter
$E_1 = \frac{E_a}{\widetilde{\psi}_\infty k_1^*}$	Activation energy parameter	$R_N = \frac{16\sigma^*\widetilde{\psi}_\infty^3}{3\alpha^*\left(\rho c_p\right)_f k^*}$	Solar radiation parameter
$\varsigma_1 = \frac{\left(\widetilde{\psi}_w - \widetilde{\psi}_\infty\right)\alpha_2}{\alpha_1}$	Quadratic convection parameters for temperature	$Re_{\tilde{x}} = \frac{\widetilde{A}_w\, L}{\nu}$	Reynolds numbers
$\omega_a = NN_3\sqrt{\frac{\widetilde{A}_0}{2\nu L}}$	Velocity slip parameters	$\omega_b = N3\mu\sqrt{\frac{\widetilde{A}_0}{2\nu L}}$	Velocity slip parameters
$K_R = \frac{L\Omega_0}{\widetilde{A}_0}$	Rotation parameter	$\lambda_a = \frac{Gr_{\tilde{x}}}{Re_{\tilde{x}}^2}$	Mixed convection parameter
$\omega_d = d_4\sqrt{\frac{\widetilde{A}_0}{2\nu L}}$	Dimensionless concentration jump parameter	$Nb = \frac{\tau D_B\left(\widetilde{\phi}_w - \widetilde{\phi}_\infty\right)}{\nu}$	Brownian motion parameter

3 Gradients

The skin friction coefficients along $\tilde{x}$ and $\tilde{y}$ directions are:

$$C_{f\tilde{x}} = \frac{2\tau_{\tilde{z}\tilde{x}}}{\rho_f \widetilde{A}_{\mathrm{w}}^2}, \text{and } C_{f\tilde{y}} = \frac{2\tau_{\tilde{z}\tilde{y}}}{\rho_f \widetilde{B}_{\mathrm{w}}^2}, \tag{14}$$

where $\tau_{\tilde{z}\tilde{x}} = \mu_f \left(1 + \frac{1}{\beta}\right) \left[\frac{\partial \tilde{A}}{\partial \tilde{z}}\right]_{\tilde{z}=0}$ and $\tau_{\tilde{z}\tilde{y}} = \mu_f \left(1 + \frac{1}{\beta}\right) \left[\frac{\partial \tilde{B}}{\partial \tilde{z}}\right]_{\tilde{z}=0}$ are the wall shear stresses.

The Nusselt number ($Nu_{\tilde{x}}$) and Sherwood number ($Sh_{\tilde{x}}$) are expressed as:

$$Nu_{\tilde{x}} = \frac{\widetilde{X} q_{\mathrm{w}}}{k\left(\widetilde{\psi}_{\mathrm{w}} - \widetilde{\psi}_{\infty}\right)}, \text{and } Sh_{\tilde{x}} = \frac{\widetilde{x}_{j_{\mathrm{w}}}}{D_B\left(\widetilde{\phi}_{\mathrm{w}} - \widetilde{\phi}_{\infty}\right)}. \tag{15}$$

By employing equation (8), the equations (14) and (15) are written as:

$$\begin{aligned} C_{f\tilde{x}} \sqrt{\frac{Re_{\tilde{x}}}{2}} &= \left(1 + \frac{1}{\beta}\right) h''(0), \\ C_{f\tilde{y}} \sqrt{\frac{Re_{\tilde{y}}}{2}} &= \left(1 + \frac{1}{\beta}\right) g''(0), \\ Nu_{\tilde{x}} \frac{L}{\widetilde{x}} \sqrt{\frac{2}{Re_{\tilde{x}}}} &= -\left[1 + R_N\left\{1 + (\chi_r - 1)\chi\right\}^3\right] \chi'(0), \\ &\text{and} \\ \mathrm{Sh}_{\tilde{x}} \frac{L}{\widetilde{x}} \sqrt{\frac{2}{Re_{\tilde{x}}}} &= -\zeta'(0). \end{aligned} \tag{16}$$

Here, $Re_{\tilde{x}} = \frac{\widetilde{A}_{\mathrm{w}} L}{\nu}$ and $Re_{\tilde{y}} = \frac{\widetilde{B}_{\mathrm{w}} L}{\nu}$ are the Reynolds numbers along $\tilde{x}$ and $\tilde{y}$ directions, respectively.

4 Computational solution procedure

4.1 Application of Gegenbauer wavelets collocation-based techniques

Recently, several changes have been made to techniques that utilize wavelets. This current study focuses on presenting a novel enhancement to the original Gegenbauer wavelet techniques (GWT) via including the principles of the Galerkin Scheme. The major benefit of the proposed techniques, in comparison to the GWT, lies in their ability to reduce the amount of computational effort required. The novel proposed techniques are easy, direct, and accessible to users. The process includes the following steps:

First step. Begin via considering the equations (9)–(11):

$$\begin{aligned} (\mathrm{h} + \mathrm{g})\,\mathrm{h}'' - 2\left(\mathrm{h}' + \mathrm{g}'\right)\mathrm{h}' + \left(1 + \frac{1}{\beta}\right)\mathrm{h}''' + 4K_R \mathrm{g}' + \frac{M}{\left(\alpha_e^2 + \xi_a^2\right)}\left(\xi_a \mathrm{g}' - \alpha_e \mathrm{h}'\right) + \\ 2\lambda_a \chi\left(1 + \varsigma_1 \chi\right) + 2\lambda_a \mathrm{N}^* \zeta\left(1 + \varsigma_2 \zeta\right) = 0, \end{aligned} \tag{17}$$

$$(\mathrm{h} + \mathrm{g})\,\mathrm{g}'' - 2\left(\mathrm{h}' + \mathrm{g}'\right)\mathrm{g}' + \left(1 + \frac{1}{\beta}\right)\mathrm{g}''' - 4K_R \mathrm{h}' - \frac{M}{\left(\alpha_e^2 + \xi_a^2\right)}\left(\xi_a \mathrm{h}' + \alpha_e \mathrm{g}'\right) = 0, \tag{18}$$

$$\frac{1}{\mathrm{Pr}}\chi'' + \frac{R_N\left\{1 + (\mathrm{X_r} - 1)\,\mathrm{X}\right\}^2}{\mathrm{Pr}}\left[(\chi_r - 1)\chi'^2 + \left\{1 + (\chi_r - 1)\,\mathrm{X}\right\}\chi''\right] + (\mathrm{h} + \mathrm{g})\chi' - n\left(h' + g'\right)\chi + Nt\chi'^2 + Nb\chi' Z' + \left(1 + \cdot\right. \tag{19}$$

$$\zeta'' - nS_c\left(h' + g'\right)\zeta + S_c\left(h + g\right)\zeta' + \frac{Nt}{Nb}\chi'' - K_R S_c \zeta\left(1 + (\chi_r - 1)\chi\right)^{n^*} \exp\left[-\frac{E_1}{(1 + (\chi_r - 1)\chi)}\right] = 0, \tag{20}$$

Second step. The proposed trial solutions from the original GWT for investigating the numerical solutions to the problem defined via equations (17–(20) are presented as follows:

$$h'(\vartheta) = \sum_{r=1}^{2^{p-1}} \sum_{b=0}^{z-1} \lambda_{r,b}^{1} \Omega_{r,b}(\vartheta) = \mathscr{R}_1^{\mathfrak{I}}\, \Omega(\vartheta), g'(\vartheta) = \sum_{r=1}^{2^{p-1}} \sum_{b=0}^{z-1} \lambda_{r,b}^{2} \Omega_{r,b}(\vartheta) = \mathscr{R}_2^{\mathfrak{I}}\, \Omega(\vartheta), \tag{21}$$

$$\chi(\vartheta) = \sum_{r=1}^{2^{p-1}} \sum_{b=0}^{z-1} \lambda_{r,b}^{3} \Omega_{r,b}(\vartheta) = \mathscr{R}_3^{\mathfrak{I}}\, \Omega(\vartheta), \tag{22}$$

$$\zeta(\vartheta) = \sum_{r=1}^{2^{p-1}} \sum_{b=0}^{z-1} \lambda_{r,b}^{4} \Omega_{r,b}(\vartheta) = \mathscr{R}_4^{\mathfrak{I}}\, \Omega(\vartheta). \tag{23}$$

The matrices $\mathscr{R}_1^{\mathfrak{I}}$, $\mathscr{R}_2^{\mathfrak{I}}, \mathscr{R}_3^{\mathfrak{I}}$, and $\mathscr{R}_4^{\mathfrak{I}}$ and $\Omega(\vartheta)$ mentioned above are provided as follows: $\mathscr{R}_i = \left[\lambda_{1,0}^{r}, \lambda_{1,1}^{r}, \lambda_{1,2}^{r}\right]^{\mathfrak{I}}$, r = 1, 2, 3. The previously mentioned solutions ((21)–(23) can be rewritten as follows:

$$\widetilde{h}'(\vartheta) = \eta_1^{\mathfrak{I}} \Pi(\vartheta), \widetilde{g}'(\vartheta) = \eta_1^{\mathfrak{I}} \Pi(\vartheta), \widetilde{\chi}(\vartheta) = \eta_4^{\mathfrak{I}} \Pi(\vartheta), \widetilde{\zeta}(\vartheta) = \eta_4^{\mathfrak{I}} \Pi(\vartheta) \tag{24}$$

The subsequent expressions were derived via substituting the relations presented in the above expression to obtain:

$$\begin{aligned}
&\widetilde{f}'(\vartheta) = \sum_{q=0}^{p} \widetilde{\lambda}_q^{1} \vartheta^q, \\
&\widetilde{g}'(\vartheta) = \sum_{q=0}^{p} \widetilde{\lambda}_q^{2} \vartheta^q, \\
&\widetilde{\chi}(\vartheta) = \sum_{q=0}^{p} \widetilde{\lambda}_q^{3} \vartheta^q, \\
&\text{And} \\
&\widetilde{\zeta}(\vartheta) = \sum_{q=0}^{p} \widetilde{\lambda}_q^{4} \vartheta^q.
\end{aligned} \tag{25}$$

Step three. The subsequent equations were derived by applying the previously mentioned simplified trial solutions to Equations (9)–(11):

$$\begin{aligned}
&\left(\widetilde{\mathrm{h}} + \widetilde{g}\right)\widetilde{\mathrm{h}}'' - 2\left(\widetilde{\mathrm{h}}' + \widetilde{g}'\right)\widetilde{\mathrm{h}}' + \left(1 + \frac{1}{\beta}\right)\widetilde{\mathrm{h}}''' + 4K_R\widetilde{g}' + \frac{M}{(\alpha_e^2 + \xi_a^2)}\left(\xi_a\widetilde{g}' - \alpha_e\widetilde{\mathrm{h}}'\right) + \\
&2\lambda_a\chi\left(1 + \varsigma_1\chi\right) + 2\lambda_a \mathrm{N}^*\zeta\left(1 + \varsigma_2\zeta\right) = 0,
\end{aligned} \tag{26}$$

$$\left(\widetilde{\mathrm{h}} + \widetilde{g}\right)\widetilde{\mathrm{h}}'' - 2\left(\widetilde{\mathrm{h}}' + \widetilde{g}'\right)\widetilde{g}' + \left(1 + \frac{1}{\beta}\right)\widetilde{g}''' - 4K_R\widetilde{h}' - \frac{M}{(\alpha_e^2 + \xi_a^2)}\left(\xi_a\widetilde{h}' + \alpha_e\widetilde{g}'\right) = 0, \tag{27}$$

$$\frac{1}{\mathrm{Pr}}\widetilde{\chi}'' + \frac{R_N\{1+(\mathrm{X_r}-1)\,\mathrm{X}\}^2}{\mathrm{Pr}}\left[(\chi_r-1)\,\widetilde{\chi}'^2 + \{1+(\chi_r-1)\,\widetilde{\chi}\}\,\widetilde{\chi}''\right] + \left(\widetilde{\mathrm{h}}+\widetilde{g}\right)\widetilde{\chi}' - n\left(\widetilde{\mathrm{h}}+\widetilde{g}\right)\widetilde{\chi} + Nt\widetilde{\chi}'^2 + Nb\chi'\mathrm{Z}' + \left(1+ \tag{28}$$

$$\widetilde{\zeta}'' - nS_c\left(\widetilde{\mathrm{h}}+\widetilde{g}\right)\widetilde{\zeta} + S_c\left(\widetilde{\mathrm{h}}+\widetilde{g}\right)\widetilde{\zeta}' + \frac{Nt}{Nb}\widetilde{\chi}'' - K_R S_c\widetilde{\zeta}(1+(\chi_r-1)\,\widetilde{\chi})^{n^*}\ \exp\left[-\frac{E_1}{(1+(\chi_r-1)\,\widetilde{\chi})}\right] = 0. \tag{29}$$

To analyze the constants denoted by $\widetilde{\lambda}_0', \widetilde{\lambda}_1', \widetilde{\lambda}_3'$, r = 1, 2, 3, we must create a system of algebraic equations. To achieve this, we will employ the specified collocation points to align and solve the equations numbered (26)–(29), as outlined.

$$\vartheta_\vartheta = \frac{p}{q-4}\vartheta_\infty, p = 1,2,3,\mathrm{q}-3, \vartheta_\vartheta = \frac{p}{q-3}\vartheta_\infty, p = 1,2,3,\mathrm{q}\ -3, \vartheta_\vartheta = \frac{m}{N-2}\vartheta_\infty, p = 1,2,3,\mathrm{q}-2$$
$$\vartheta_\vartheta = \frac{m}{N-2}\vartheta_\infty, p = 1,2,3,\mathrm{q}\ -\ 3 \tag{30}$$

Fourth step. By solving the aforementioned system of algebraic equations, the values of the variables denoted by $\widetilde{\lambda}'s$ are determined. Subsequently, these values are substituted into Equations (17–(20) to obtain the corresponding results. Finally, by inserting these values into Equations ((9)–(11), the complete solution to the problem is derived.

4.2 Code authentication

Table 2 is the validation table for the current work with the existing literature. The outcomes will best match each other.

alt-text: Table 2

Table 2

The table layout displayed in this section is not how it will appear in the final version. The representation below is solely purposed for providing corrections to the table. To view the actual presentation of the table, please click on the Preview located at the top of the page.

Comparison of $Nu_{\widetilde{x}}$ values across different A_v and n parameters.

A_v	0.5	0.5	1.0	1.0
n	0.0	5.0	0.0	5.0
Result (Nandi et al., 2024)	2.2616329726	7.2233092508	2.6115096686	8.3407636409
Result (Ibrahim & Anbessa, 2020)	2.2616208431	7.2233049205	2.6114948052	8.3407540806
Result (Krishna, 2020)	2.2616092689	7.2232801587	2.6114815046	8.3407255264
Present study	2.2616208431	7.2233049205	2.6114948052	8.3407540806

5 Results and interpretations

The analysis outcome of the two-phase nanofluid materials for rotating Casson flow and the propagation of solar radiation mechanism over an exponentially elongating sheet with Hall current and ion slip effects are explained in detail in this section. The results demonstrate the impact of different crucial factors on the temperature $\chi(\vartheta)$, concentration $\zeta(\vartheta)$, and velocity $(\mathrm{h}'(\vartheta)\ g'(\vartheta))$. The range of controlling parameters are Casson parameters ($\beta = 0.2, 0.3, 0.4$), Hall current parameter (ξ_a = 1.0, 1.5, 2.0) and ion slip parameter ($\xi_b = 0.2, 0.4, 0.6$), Solar radiation parameter (R_N = 2.0, 4.0, 6.0), Rotation parameter ($K_R = 2, 4, 6$), Magnetic field (M 0.2, 0.4, 0.6), Eckert number ($\mathrm{E_c} = 3.0, 5.0, 7.0$), dimensionless temperature jumps parameters ($\omega_c = 2, 3, 4$). Table 3 demonstrates the thermal energy transport rate through

computational processes. Additionally, the tables illustrate how the physical quantity $Nu_{\bar{x}}$ responds to the governing operational parameter.

alt-text: Table 3

Table 3

The table layout displayed in this section is not how it will appear in the final version. The representation below is solely purposed for providing corrections to the table. To view the actual presentation of the table, please click on the Preview located at the top of the page.

Computed values of $Nu_{\bar{x}}$.

Parameters	Values	$Nu_{\bar{x}}$	Thermal transport rate effect
M	0.2	2.31852	This M parameter reduces the rate of heat transport on the elongating surface sheet.
	0.4	2.28131	
	0.6	2.14287	
R_N	2.0	2.14718	This solar radiation parameter positively affects the thermal energy transport rate.
	4.0	2.47419	
	6.0	2.77869	
ω_c	2	2.27338	This ω_c parameter has an increasing effect on the surface boundary and the rate of heat transport
	3	2.35077	
	4	2.48723	
Nt	0.2	2.29319	This Nt parameter has a dropping impact on the heat flow rate across the elongating surface sheet.
	0.3	2.24672	
	0.4	2.17120	

Casson parameter (β): A Casson parameter (β) is characterized as a shear-thinning fluid that exhibits infinite viscosity when there is no shear rate. It also possesses yield stress, demonstrating that flow will not occur unless this stress is surpassed. Moreover, at infinitely high shear rates, the viscosity of the liquid approaches zero. Fig. 2a shows that as the β rises, both the $h'(\vartheta)$ and $g'(\vartheta)$ reduce. This is because a greater yield stress produces a larger resistance to flow, which reduces the speed of the fluid. Also, an increase in the intensity β parameter indicates a larger yield stress, demonstrating that a higher force is required to start the flow of the fluid. Therefore, for any given shear stress, a liquid with a greater β parameter will show a decrease in both $h'(\vartheta)$ and $g'(\vartheta)$. Physically, honey shows a larger yield stress compared to water, demanding a higher amount of force to start its movement. Therefore, as honey starts to flow, it happens to be less viscous; nonetheless, it will never attain the same smoothness as water. This performance is displayed in Fig. 2a.

Images may appear blurred during proofing as they have been optimized for fast web viewing. A high quality version will be used in the final publication. Click on the image to view the original version.

alt-text: Fig. 2a

Fig. 2a

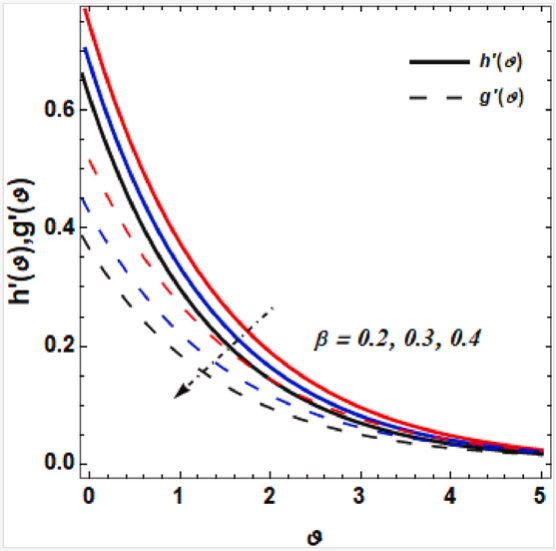

Influence of β on $h'(\vartheta)$.

Hall current parameter (ξ_a), ion slip parameter (ξ_b), and Rotation parameter (K_R): The ξ_a parameter is a quantity of dimension employed in magnetohydrodynamics (MHD) to illustrate how ξ_a impact the movement of electrically conductive fluids, containing fluid metals and plasmas, when exposed to a magnetic field. Fig. 2b demonstrates the $h'(\vartheta)$ for different values of the ξ_a parameter. The Fig. 2b indicates that $h'(\vartheta)$ raise as the values of ξ_a rise up. However, as the ξ_a raises, it shows a greater impact of the Hall effect on the fluid flow. As the ξ_a rise up, it indicates that the magnetic field has a larger effect on the charged particles. This generates a Lorentz force that affects the charged particles in the fluid, resulting in their movement in a direction that is perpendicular to both the current and the magnetic field. The $h'(\vartheta)$ with different values of various values of the ξ_b parameter are shown in Fig. 2c. An elevated ξ_b parameter characteristically shows stronger electric forces influencing the liquid. These electric forces can speed up the liquid particles, thereby contributing to an increased $h'(\vartheta)$. Physically, there is an inverse correlation between the ion slip parameter and the Lorentz force. Therefore, this leads to an increase in speed distribution $h'(\vartheta)$. A K_R parameter is a measure that explains the rotational characteristics of a fluid system. The effect of the K_R parameter on the $h'(\vartheta)$ is shown in Fig. 2d it was observed that the $h'(\vartheta)$ is elevated across the entire boundary layer region.

Images may appear blurred during proofing as they have been optimized for fast web viewing. A high quality version will be used in the final publication. Click on the image to view the original version.

alt-text: Fig. 2b

Fig. 2b

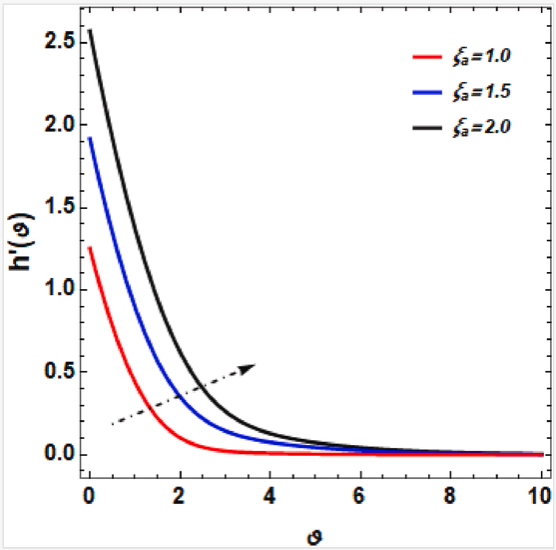

Influence of ξ_a on $h'(\vartheta)$.

Images may appear blurred during proofing as they have been optimized for fast web viewing. A high quality version will be used in the final publication. Click on the image to view the original version.

alt-text: Fig. 2c

Fig. 2c

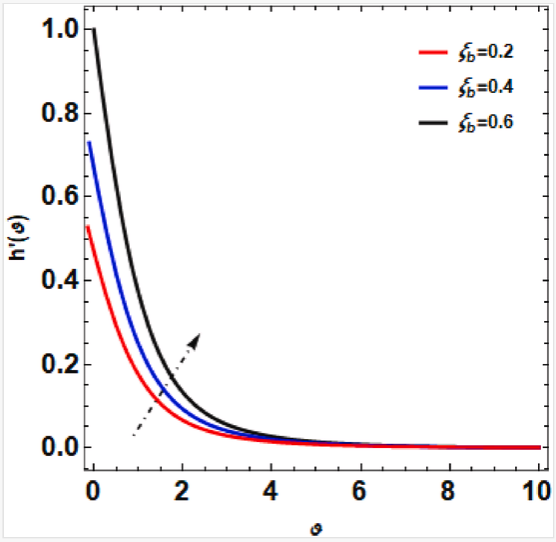

Influence of ξ_b on $h'(\vartheta)$.

Images may appear blurred during proofing as they have been optimized for fast web viewing. A high quality version will be used in the final publication. Click on the image to view the original version.

alt-text: Fig. 2d

Fig. 2d

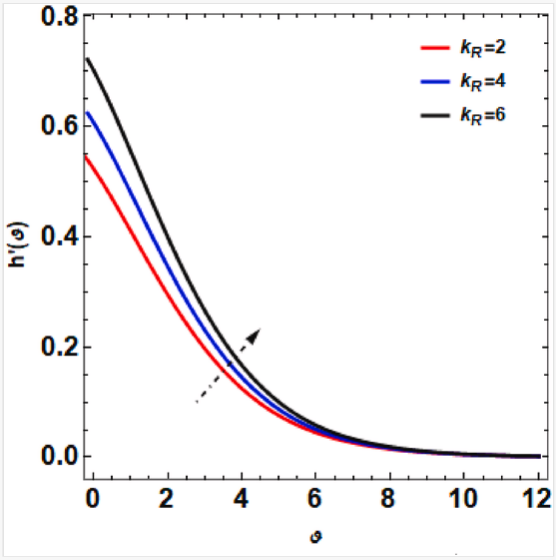

Influence of K_R on $h'(\vartheta)$.

Magnetic field (M): The magnetic field reduces the velocity profile in a fluid flow due to the phenomenon known as magnetohydrodynamic (MHD) drag. When a magnetic field is applied to a conducting fluid (such as a plasma, liquid metal, or electrically conducting nanofluid), it induces a Lorentz force. This force is a product of the interaction between the magnetic field and the electric currents generated in the fluid. The Lorentz force acts perpendicular to both the magnetic field and the direction of fluid flow, creating a resistive force that opposes the motion of the fluid. The presence of the magnetic field introduces additional resistive forces within the fluid. These forces act against the fluid's motion, leading to a reduction in the fluid's velocity. The stronger the magnetic field, the greater the resistive force, and thus, the more significant the reduction in velocity (see Fig. 2e).

alt-text: Fig. 2e

Fig. 2e

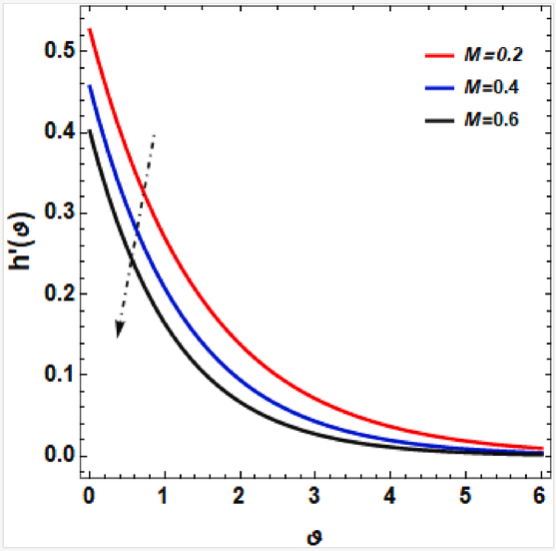

Impact of M on $\mathrm{h}'(\vartheta)$.

Solar radiation parameter (R_N) and heat generation parameter (Q_N): Thermal radiation increases the temperature profile due to the energy transfer that occurs when radiation is absorbed by the material (see Fig. 3a). When thermal radiation interacts with a material, it is absorbed by the particles within that material. This absorption of radiation energy increases the internal energy of the particles, which manifests as an increase in temperature. The absorbed radiation causes an increase in thermal energy within the material. This energy contributes to the overall temperature, especially in cases where radiation is significant compared to other forms of heat transfer. The heat generation parameter Q_N is a non-dimensional value that measures the rate of heat creation in a fluid system. It is estimated as the ratio of the heat production rate to the thermal conductivity of the substance. The Q_N acts as an effective tool in comprehending and designing thermal transport in fluid systems. It enables calculating temperature distribution within a system, determining heat flux at a surface, and evaluating the necessary cooling capacity for a given system. This performance is shown in Fig. 3b.

alt-text: Fig. 3a

Fig. 3a

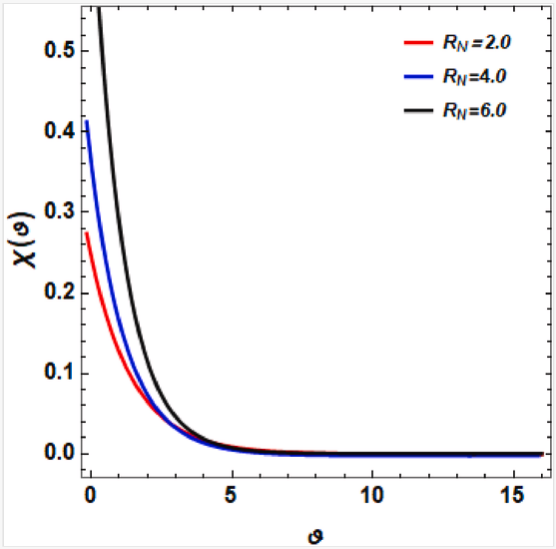

Impact of R_N on $\chi(\vartheta)$.

alt-text: Fig. 3b

Fig. 3b

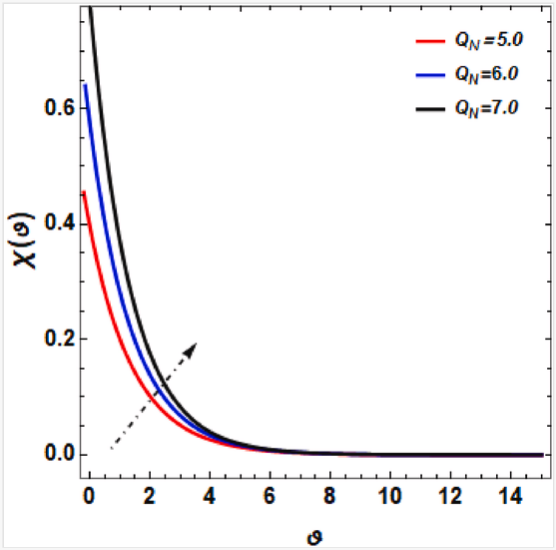

Impact of ω_c on $\chi(\vartheta)$.

Eckert number (E_c) and Dimensionless temperature jumps parameters (ω_c): The E_c is a dimensionless parameter in fluid dynamics, that calculates the correlation between kinetic energy and enthalpy transport. It is usually utilized in the research of thermal transport in high-speed flows. The ratio between the kinetic energy density and the thermal energy density is a vital factor in determining the equilibrium between these two energy types within the flow. Fig. 3c

shows the influence of E_c on the $\chi(\vartheta)$. The flow is regulated via kinetic energy when the E_c is high, showing that kinetic energy is dominant over thermal energy. A low E_c indicates that the fluid has a substantially higher amount of thermal energy compared to its kinetic energy. By inspecting the procedure of solar radiation heating the fluid, we can gain an understanding of the fundamental reasons for this performance. When the fluid absorbs solar radiation, it experiences a temperature rise, leading to an increment. Therefore, the fluid gains extra kinetic energy, resulting in increased motion. Physically, The E_c plays a vital role in improving thermal control devices across numerous engineering fields, including automotive industries electronics cooling, and marine and biomedical engineering. Hence, when there is a higher level of heat dissipation caused by viscosity, it leads to an increase in fluid temperature. The effect of the ω_c on the $\chi(\vartheta)$ is shown in Fig. 3d. It can be observed that $\chi(\vartheta)$ declines throughout the thermal boundary layer region as the values of ω_c Strengthen.

Images may appear blurred during proofing as they have been optimized for fast web viewing. A high quality version will be used in the final publication. Click on the image to view the original version.

alt-text: Fig. 3c

Fig. 3c

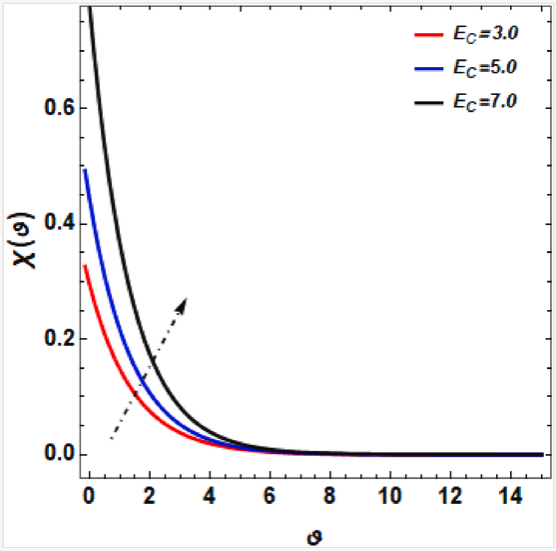

Influence of E_c on $\chi(\vartheta)$.

Images may appear blurred during proofing as they have been optimized for fast web viewing. A high quality version will be used in the final publication. Click on the image to view the original version.

alt-text: Fig. 3d

Fig. 3d

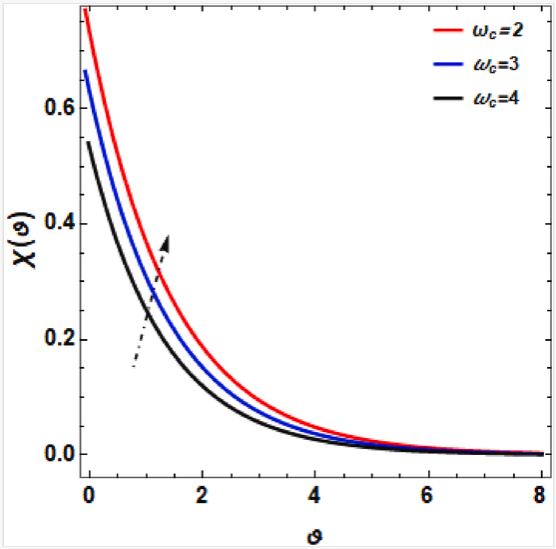

Effect of ω_c on $\chi(\vartheta)$.

Activation energy parameter (E_1) and Solutal slip parameter (ω_d): In the Arrhenius model of reaction rates, the activation energy refers to the least amount of energy required for reactants to undergo a chemical reaction (CR). The E_1 affects the $\zeta(\vartheta)$ by influencing the rate at which CR occurs (see Fig. 4a). The rate of CR is exponentially dependent on the E_1 as illustrated via the Arrhenius formula $\left(exp\left(-\frac{E_a}{k_1^*\widetilde{\psi}}\right)\right)$. With a higher activation energy, the reaction rate increases exponentially. The E_1 parameter normally varies with temperature. Therefore, a rise in E_1 relates to an increase in the effective temperature of the system. Fig. 4b illustrates the effect of the ω_d on the concentration profile of nanoparticles. For increasing values of E_1, the $\zeta(\vartheta)$ is decreased.

Images may appear blurred during proofing as they have been optimized for fast web viewing. A high quality version will be used in the final publication. Click on the image to view the original version.

alt-text: Fig. 4a

Fig. 4a

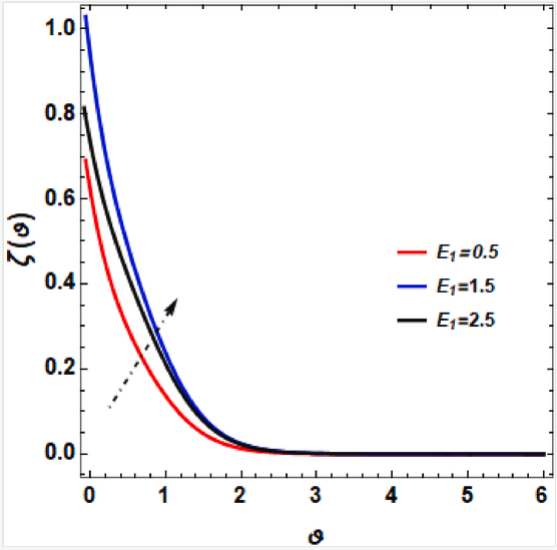

Impact of ω_d on $\zeta(\vartheta)$.

Images may appear blurred during proofing as they have been optimized for fast web viewing. A high quality version will be used in the final publication. Click on the image to view the original version.

alt-text: Fig. 4b

Fig. 4b

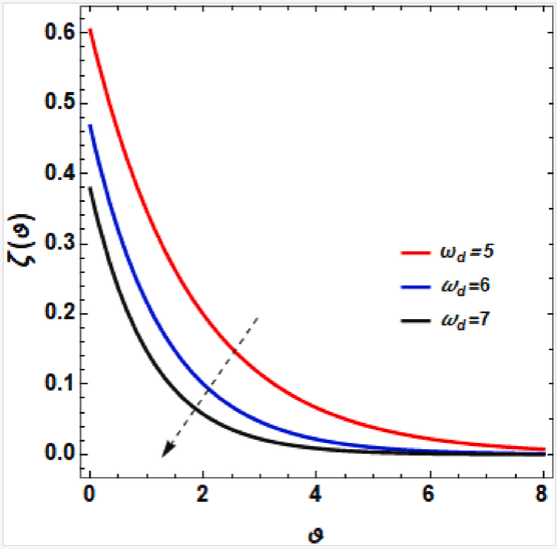

Impact of ω_d on $\zeta(\vartheta)$.

Fig. 5a displays the various curves for different values of a Casson parameter, ion slip parameter, and magnetic field on skin friction. it revealed that an increase in the ion slip parameter and Casson parameter leads to a reduction in the skin friction $\left(1+\frac{1}{\beta}\right)h''(0)$. Also, the solar radiation, Eckert number, and dimensionless temperature jump parameter enhance the rate of $-\left[1+Rd\left\{1+(\chi_r-1)\chi\right\}^3\right]\chi'(0)$ (see Fig. 5b).

Images may appear blurred during proofing as they have been optimized for fast web viewing. A high quality version will be used in the final publication. Click on the image to view the original version.

alt-text: Fig. 5a

Fig. 5a

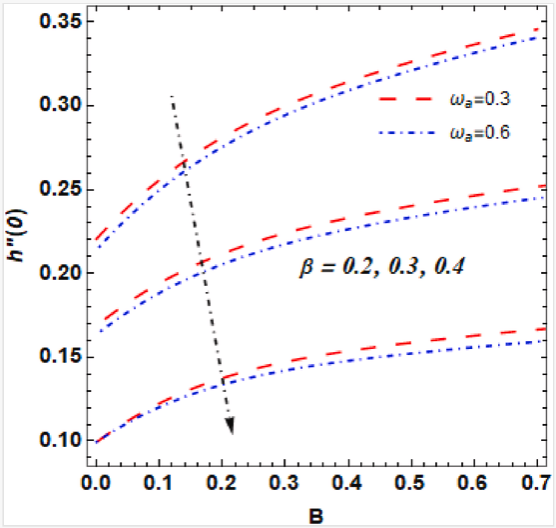

Outcome of β on $h''(0)$.

Images may appear blurred during proofing as they have been optimized for fast web viewing. A high quality version will be used in the final publication. Click on the image to view the original version.

alt-text: Fig. 5b

Fig. 5b

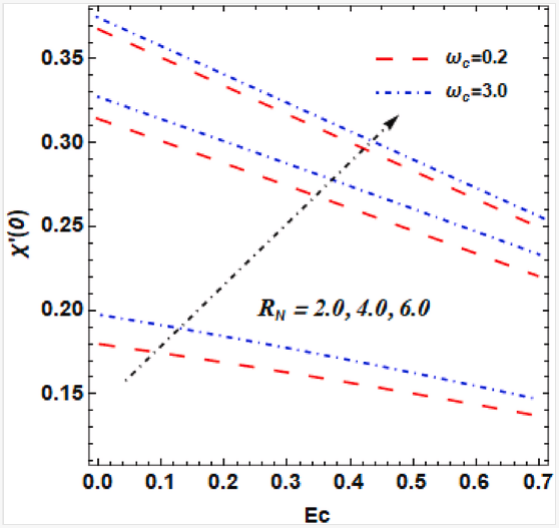

Outcome of R_N on heat transfer rate.

Final remarks

In conclusion, this present research introduces a novel method to inspect the influence of multiple slip conditions and propagation of incompressible Casson nanofluid flow in exponentially elongating sheets with hall current and ion slip effects using Gegenbauer wavelets collocation-based techniques. This structure has various implications in server fields such as thermal energy storage, space exploration, high temperature, and polymer processes. It is generally utilized in this area for many purposes. The key findings of this study are outlined below.

- The Hall current parameter and ion slip parameter accelerate the flow momentum.
- Flow momentum is accelerated with the rotation parameter, whereas the opposite effect is observed for the magnetic parameter.
- The solar thermal radiation, heat generation parameter increases the thermal energy.
- The rising value of the Eckert number intensified the temperature field.
- The concentration field is boosted by the activation energy parameter and the solutal slip parameter.
- Temperature jumps parameters support the improvement in heat propagation.
- Surface drag force is enhanced to reduce values of the Casson parameter and velocity slip condition.
- As the values of solar radiation increase, the heat transfer rate shows an improvement.

Future recommendation

Future research could extend the parametric study to explore the effects of different fluid properties e.g., nanoparticle shapes on the flow dynamics. Investigating the nonlinear effects and performing a stability analysis of the flow could provide deeper insights into the behavior of the system under extreme conditions, which is critical for high-performance industrial applications. To solidify the theoretical findings, experimental studies should be conducted, especially focusing on real-world applications such as MHD generators and thermal energy storage systems.

Data availability statement

The datasets used and/or analyzed during the current study are available from the corresponding author upon reasonable request.

Conflicts of interest

The authors declare no conflict of interest.

CRediT authorship contribution statement

Mohammad Akram: Conceptualization, Data curation, Software, Validation, Writing – review & editing. **Osama Ala'yed:** Conceptualization, Data curation, Software, Validation, Writing – review & editing. **Rania Saadeh:** Writing – original draft, Validation, Software, Methodology, Formal analysis, Conceptualization. **Ahmad Qazza:** Conceptualization, Data curation, Software, Validation, Writing – review & editing. **A.M. Obalalu:** Writing – original draft, Validation, Software, Methodology, Formal analysis, Conceptualization. **Umair Khan:** Writing – review & editing, Writing – original draft, Validation, Supervision, Conceptualization. **Adil Darvesh:** Writing – original draft, Visualization, Validation, Investigation, Data curation. **A.A. Usman:** Writing – original draft, Visualization, Validation, Investigation, Data curation. **A.M. Abdul-Yekeen:** Writing – original draft, Visualization, Validation, Investigation, Data curation. **Syed Modassir Hussain:** Writing – review & editing, Validation, Software, Project administration, Funding acquisition.

Acknowledgment

This work was funded by the Deputyship of Research & Innovation, Ministry of Education in Saudi Arabia, through project number: Research Group Project-1, No. 763. In addition, the authors would like to express their appreciation Q4 for the support provided by the Islamic University of Madinah.

References

The corrections made in this section will be reviewed and approved by a journal production editor. The newly added/removed references and its citations will be reordered and rearranged by the production team.

Ahmed, J., Bourazza, S., Sarfraz, M., Orsud, M.A., Eldin, S.M., Askar, N.A., & Elkotb, M.A. (2023). Heat transfer in Jeffrey fluid flow over a power law lubricated surface inspired by solar radiations and magnetic flux. Case Studies in Thermal Engineering, 49, 103220.

Ahmed, A., Khan, M., Sarfraz, M., Ahmed, J., & Iqbal, Z. (2021). Forced convection in 3D Maxwell nanofluid flow via Cattaneo–Christov theory with Joule heating. Proceedings of the Institution of Mechanical Engineers - Part E: Journal of Process Mechanical Engineering, 235(4), 747–757.

Al-Turef, G.A., Obalalu, A.M., Saleh, W., Shah, S.H.A.M., Darvesh, A., Khan, U., … Hussain, S.M. (2024). Computational study and application of the Hamilton and crosser model for ternary hybrid nanofluid flow past a Riga wedge with heterogeneous catalytic reaction. Nano, 2450105.

Butt, Z.I., Ahmad, I., Hussain, S.I., Raja, M.A.Z., Shoaib, M., & Ilyas, H. (2024). Intelligent computing paradigm for unsteady magneto nano-polymeric Casson nanofluid with Ohmic dissipation and thermal radiation. Chinese Journal of Physics, 88, 212–269.

Gasmi, H., Obalalu, A.M., Akindele, A.O., Salaudeen, S.A., Khan, U., Ishak, A., & Abed, A.M. (2024). Thermal performance of a motile microorganism within the two-phase nanofluid flow for the distinct non-Newtonian models on static and moving surfaces. Case Studies in Thermal Engineering, 104392.

Gasmi, H., Obalalu, A.M., Kaswan, P., Khan, U., Ojewola, O.B., Abdul-Yekeen, A.M., & Abed, A.M. (2024). Features of melting heat transfer in magnetized squeezing radiative flow of ternary hybrid nanofluid.

Case Studies in Thermal Engineering, 61, 104842.

Hall, D. (1988). Measurements of the mean force on a particle near a boundary in turbulent flow. Journal of Fluid Mechanics, 187, 451–466.

Ibrahim, W., & Anbessa, T. (2020). Mixed convection flow of a Maxwell nanofluid with Hall and ion slip impacts employing the spectral relaxation method. Heat Transf, 49(5), 3094–3118.

Kanwal, S., Shah, S.A.A., Bariq, A., Ali, B., Ragab, A.E., & Az-Zo'bi, E.A. (2023). Insight into the dynamics of heat and mass transfer in nanofluid flow with linear/nonlinear mixed convection, thermal radiation, and activation energy effects over the rotating disk. Scientific Reports, 13(1), 23031.

Khan, M., Sarfraz, M., Ahmed, J., Ahmad, L., & Ahmed, A. (2021). Viscoelastic nanofluid motion for Homann stagnation-region with thermal radiation characteristics. Proceedings of the Institution of Mechanical Engineers - Part C: Journal of Mechanical Engineering Science, 235(21), 5324–5336.

Khan, M., Sarfraz, M., Ahmed, J., Ahmad, L., & Fetecau, C. (2020). Non-axisymmetric Homann stagnation-point flow of Walter's B nanofluid over a cylindrical disk. Applied Mathematics and Mechanics, 41(5), 725–740.

Kpossa, M., & Monwanou, V. (2023). Combined effect of helical force and rotation on the double convection of a binary viscoelastic fluid in a porous medium: Linear and weakly nonlinear analysis. ZAMM-Journal of Applied Mathematics and Mechanics/Zeitschrift für Angewandte Mathematik und Mechanik, 103(12), e202200363.

Krishna, M.V. (2020). Hall and ion slip impacts on unsteady MHD free convective rotating flow of Jeffreys fluid with ramped wall temperature. Int. Commun. Heat Mass Transf., 119, 104927.

Li, S., Khan, M.I., Alzahrani, F., & Eldin, S.M. (2023). Heat and mass transport analysis in radiative time dependent flow in the presence of Ohmic heating and chemical reaction, viscous dissipation: An entropy modeling. Case Studies in Thermal Engineering, 42, 102722.

Li, S., Saadeh, R., Madhukesh, J.K., Khan, U., Ramesh, G.K., Zaib, A., … Sherif, E.S.M. (2024). Aspects of an induced magnetic field utilization for heat and mass transfer ferromagnetic hybrid nanofluid flow driven by pollutant concentration. Case Studies in Thermal Engineering, 53, 103892.

Mahmood, Z., ur Rehman, M., Khan, U., Ali, B., & Haque Siddiqui, M.I. (2024). Enhanced transport phenomena in Casson fluid flow over radiative moving surface: Influence of velocity and thermal slip conditions with mixed convection and chemical reaction. Modern Physics Letters B, 2450383.

Mebarek-Oudina, F., Chabani, I., Vaidya, H., & Ismail, A.A.I. (2024). Hybrid-nanofluid magneto-convective flow and porous media contribution to entropy generation. International Journal of Numerical Methods for Heat and Fluid Flow, 34(2), 809–836.

Mebarek-Oudina, F., Dharmaiah, G., Balamurugan, K.S., Ismail, A.I., & Saxena, H. (2023). The role of quadratic-linearly radiating heat source with Carreau nanofluid and exponential space-dependent past a cone and a wedge: A medical engineering application and renewable energy. Journal of Computational Biophysics and Chemistry, 22(8), 997–1011.

Mustafa, M., Khan, J.A., Hayat, T., & Alsaedi, A. (2017). Buoyancy effects on the MHD nanofluid flow past a vertical surface with chemical reaction and activation energy. International Journal of Heat and Mass Transfer, 108, 1340–1346.

Nandi, S., Kumbhakar, B., & Seth, G.S. (2024). Hall and ion slip effects on rotating Casson nanofluid flow past a deformable sheet with multiple slips and activation energy: Modern impressions of non-linear radiation and convection. International Journal of Algorithms, Computing and Mathematics, 10(2), 65.

Nimmy, P., Obalalu, A.M., Nagaraja, K.V., Madhukesh, J.K., Khan, U., Ishak, A., … Abdou, M.M.M. (2024). Thermal scrutinization of time-dependent flow of nanoparticles over a rotating sphere with autocatalytic chemical reaction. The European Physical Journal Plus, 139(3), 1–15.

Obalalu, A.M., Alfwzan, W.F., Memon, M.A., Darvesh, A., Adegbite, P., & Hendy, A.S. (2024). Energy optimization of quadratic thermal convection on two-phase boundary layer flow across a moving vertical flat plate. Case Studies in Thermal Engineering, 104073.

Paul, A., Sarma, N., & Patgiri, B. (2023). Thermal and mass transfer analysis of Casson-Maxwell hybrid nanofluids through an unsteady horizontal cylinder with variable thermal conductivity and Arrhenius activation energy. Numerical Heat Transfer, Part A: Applications, 1–26.

Paun, M.A., Sallese, J.M., & Kayal, M. (2013). Hall effect sensors design, integration and behavior analysis. Journal of Sensor and Actuator Networks, 2(1), 85–97.

Raja Sekhar, P., Sreedhar, S., Vijaya Kumar, P., Ibrahim, S.M., Ganteda, C., Hussain, S.M., … Markowska, K. (2024). Investigating radiative heat transfer, varied wall thickness, and slip effects on Casson nanofluid flow over a stretched sheet with heat source. International Journal of Modelling and Simulation, 1–17.

Ram, M.S., Ashok, N., Salawu, S.O., & Shamshuddin, M.D. (2023). Significance of cross diffusion and uneven heat source/sink on the variable reactive 2D Casson flowing fluid through an infinite plate with heat and Ohmic dissipation. International Journal of Modelling and Simulation, 43(4), 347–361.

Ramesh, K., Mebarek-Oudina, F., Ismail, A.I., Jaiswal, B.R., Warke, A.S., Lodhi, R.K., & Sharma, T. (2023). Computational analysis on radiative non-Newtonian Carreau nanofluid flow in a microchannel under the magnetic properties. Scientia Iranica, 30(2), 376–390.

Ramesh, K., Mebarek-Oudina, F., & Souayeh, B. (eds.). (2024b). Mathematical modelling of fluid dynamics and nanofluids. CRC Press, Taylor & Francis Group.

Ramesh, G.K., Saadeh, R., Madhukesh, J.K., Qazza, A., Khan, U., Zaib, A., … Abed, A.M. (2024). Neural network algorithms of a curved riga sensor in a ternary hybrid nanofluid with chemical reaction and Arrhenius kinetics. Journal of Radiation Research and Applied Sciences, 17(4), 101078.

Rana, P., & Khurana, M. (2023). Linear and weakly nonlinear investigation in thermal stability analyses of MHD convection utilizing non-Newtonian nanofluid in rotating frame of reference. Waves in Random and Complex Media, 1–27.

Roja, A., Saadeh, R., Kumar, R., Qazza, A., Khan, U., Ishak, A., … Pop, I. (2024). Ramification of Hall effects in a non-Newtonian model past an inclined microchannel with slip and convective boundary conditions. Applied Rheology, 34(1), 20240010.

Rout, B.R., Parida, S.K., & Panda, S. (2013). MHD heat and mass transfer of chemical reaction fluid flow over a moving vertical plate in presence of heat source with convective surface boundary condition. International Journal of Chemical Engineering, 2013.

Salawu, S.O., Obalalu, A.M., & Shamshuddin, M.D. (2023). Nonlinear solar thermal radiation efficiency and energy optimization for magnetized hybrid Prandtl–Eyring nanoliquid in aircraft. Arabian Journal for Science and Engineering, 48(3), 3061–3072.

Sarfraz, M., & Khan, M. (2024). Rheology of gyrotactic microorganisms in Jeffrey fluid flow: A stability analysis. Modern Physics Letters B, 38(5), 2450003.

Sarfraz, M., Khan, M., Ullah, M.Z., & Abuzaid, D. (2023). Significance of Buongiorno's model on viscoelastic MHD flow over a heated lubricated surface subject to Joule heating. International Journal of Modern Physics B, 37(18), 2350171.

Sharma, Y.D., & Yadav, O.P. (2023). The linear and non-linear study of effect of rotation and internal heat source/sink on Bénard convection. Fluid Dynamics Research, 55(4), 045503.

Shoaib, M., & Javed, T. (2024). MHD radiative natural convective heat transfer enhancement for Casson nanofluid flow on a horizontal circular cylinder. Journal of Computational Science, 102257.

Singh, S.P., Upreti, H., & Kumar, M. (2024). Flow and heat transfer assessment in magnetized Darcy-Forchheimer flow of Casson hybrid nanofluid through cone, wedge, and plate. BioNanoScience, 14(1), 395–408.

Ullah, A.Z., Guo, X., Gul, T., Ali, I., Saeed, A., & Galal, A.M. (2023). Thin film flow of the ternary hybrid nanofluid over a rotating disk under the influence of magnetic field due to nonlinear convection. Journal of Magnetism and Magnetic Materials, 573, 170673.

Q5 Vardagala, J., Sreedharamalle, S., Moorthi, A., Gorintla, S., & Pallavarapu, L. (2024). Hydromagnetic peristaltic flow of convective Casson nanofluid through a vertical porous channel under the influence of Ohmic heating and viscous dissipation effects. World Journal of Engineering.

Venkateswarlu, B., & Narayana, P.V.S. (2015). MHD visco-elastic fluid flow over a continuously moving vertical surface with chemical reaction. Walailak Journal of Science and Technology, 12(9), 775–783.

Vinothkumar, B., Saadeh, R., Poornima, T., Qazza, A., Sreenivasulu, P., Subba Rao, A., … Siddiqui, M.I.H. (2024). Two-phase numerical simulation of thermal and solutal transport exploration of a non-Newtonian nanomaterial flow past a stretching surface with chemical reaction. Open Physics, 22(1), 20240036.

Zeeshan, A., Awais, M., Alzahrani, F., & Shehzad, N. (2021). Energy analysis of non-Newtonian nanofluid flow over parabola of revolution on the horizontal surface with catalytic chemical reaction. Heat Transfer, 50(6), 6189–6209.

Queries and Answers

Q1

Query: Please confirm that the provided **emails** “adebowale.obalalu17@gmail.com, umairkhan@sakarya.edu.tr” are the correct address for official communication, else provide an alternate e-mail address to replace the existing one, because private e-mail addresses should not be used in articles as the address for communication.

Answer:

Q2

Query: The **country name** has been inserted for the [h] affiliation. Please check, and correct if necessary.

Answer:

Q3

Query: Please check the hierarchy of the section headings.

Answer:

Q4

Query: Have we correctly interpreted the following funding source(s) and country names you cited in your article: Deputyship of Research & Innovation, Ministry of Education in Saudi Arabia; Islamic University of Madinah,?

Answer:

Q5

Query: Please add the **volume number and page range** for the bibliography in reference Vardagala et al., 2024.

Answer:

Q6

Query: Please confirm that given names and surnames have been identified correctly and are presented in the desired order and please carefully verify the spelling of all authors' names.

Answer: